Conference paper

Zoi Salta*, Agnie M. Kosmas and Oscar N. Ventura

Kinetics and thermodynamics of the hydroxylation products in the photodegradation of the herbicide Metolachlor

https://doi.org/10.1515/pac-2018-1205

Abstract: Electronic structure calculations have been performed to determine the thermochemistry and kinetics of the reaction between OH and the radicals of the S enantiomer of the herbicide Metolachlor, 2-chloro-N-(2-methyl-6-ethylphenyl)-N(2-methoxy-1-methylethyl) acetamide (MC), produced by photoinduced breaking of the C–Cl bond. Both density functional and *ab initio* composite methods were employed to calculate the structure of reactants, intermediates, transition states and products, in gas phase and in aqueous solution. The expected relative abundance of each product was calculated and compared to the experimentally observed concentrations. It is shown that a combination of thermodynamic and kinetic characteristics interplay to produce the expected theoretical abundances, which turn out to be in agreement with the experimentally observed distribution of products.

Keywords: density functional theory; Eurasia 2018; herbicides; hydroxylation; kinetics; metolachlor; photodegradation; thermochemistry.

Introduction

Herbicides constitute a large part of the agrochemicals employed in modern extensive agriculture [1]. They and their degradation products often represent a source of contamination of surface water, eventually constituting a health threat for livestock and humans [2].

2-Chloro-N-(2-methyl-6-ethylphenyl)-N-(2-methoxy-1-methylethyl)acetamide, a member of the chloroacetanilide family, commercially known as Metolachlor (MC, Ciba-Geigy®), and obtained as a racemic mixture of R and S enantiomers [3], is one of the most commonly used herbicides. MC dechlorination occurs by the action of soil microorganisms, producing the two most important ionic degradates, MC-ESA (metolachlor ethane sulfonic acid) and MC-OA (metolachlor oxanilic acid), more mobile than MC itself and identified in many samples of running and drinking water, even in larger concentrations than the parent herbicide [4].

Non-biological photodecomposition and oxidation of MC, on the other side, lead to many species which have been also identified in surface waters [5–16]. Given its possible high environmental impact due to its extended use, numerous experimental studies have been performed on the photocatalytic oxidation under diverse environmental conditions, examining the nature and toxicity of the photoproducts [17, 18–33]. It is well established that sunlight irradiation causes the cleavage of the C–Cl bond. Radicals formed in this way react directly with available OH radicals in the medium, leading to a wide variety of products.

Article note: A collection of invited papers based on presentations at the 15th Eurasia Conference on Chemical Sciences (EuAsC2S-15) held at Sapienza University of Rome, Italy, 5–8 September 2018.

***Corresponding author: Zoi Salta,** SMART Lab, Scuola Normale Superiore di Pisa, Piazza dei Cavalieri, 7, 56126 Pisa, Italy, e-mail: Zoi.Salta@sns.it. https://orcid.org/0000-0002-7826-0182
Agnie M. Kosmas: Physical Chemistry Sector, Department of Chemistry, University of Ioannina, Ioannina 45110, Greece. https://orcid.org/0000-0003-4089-6254
Oscar N. Ventura: Computational Chemistry and Biology Group, CCBG, DETEMA, Facultad de Química, Udelar, Montevideo, Uruguay. https://orcid.org/0000-0001-5474-0061

Although OH radicals would not be directly produced by irradiation under sunlight conditions, photosensitizers in the media can help to produce them. It is well known that chromophoric dissolved organic matter, nitrite and nitrate anions, as well as iron hydroxides (through Fenton reactions) produce OH radicals in surface waters [34]. The mechanism is well understood only in the case of nitrite and nitrate anions [35], but the presence of OH radicals is well documented. A review of the presence of the OH radical in the environment, including surface waters, can be found in ref. [36].

The hydroxylation mechanism appears to be the major oxidation channel in most investigations, yielding mono-hydroxylated species. Some other studies however, have found the formation of chloroacetic acid, morpholinone derivatives and several cyclization products [17]. It seems clear that depending on the environmental conditions (amount of radiation, presence of photosensitizers, temperature, etc.) hydroxylation mechanisms may be the most important reaction channel. In this work however, we have focused in the study of the derivatives observed when photodegradation initiated by the breaking of the C–Cl bond is the main reaction channel.

In a previous work [37] we determined computationally the structure of the different conformers of MC, the radical structures obtained by photochemical breaking of the C–Cl bond and the most important, experimentally identified mono-hydroxylated photofragmentation products. The conformational study yielded good agreement with the available experimental data for rotational barriers. Reaction enthalpies for the various hydroxylation pathways were then calculated. Based on these values, a theoretical justification of the significance of the various hydroxylation channels was suggested, with particular attention to the importance of the phenyl group hydroxylation. Thermochemistry arguments however, were unable to explain fully the experimentally observed relative abundance of the products. Therefore, in this work we determined the structure and energies of the transition states connecting the most stable MC radical with the different mono-hydroxylated compounds in order to discuss more completely the likeliness of the different mechanisms leading to the products. The results show that the experimental relative abundance is caused by a combination of kinetic and thermodynamic factors which affect differently the reaction profiles of the species.

Methods

MC parent species is shown in Fig. 1. It presents several elements of symmetry, of which the most prominent is the 1'C position where enantiomerism gives rise to the two enantiomers *R* and *S* [41–44]. Only the *S* enantiomer is biologically active.

MC possesses also an axis of isomerization, around which two conformers (αR) and (αS) are possible. It is generally found that in ortho substituted phenyl groups, steric effects preclude free rotation around the amide C–N bond causing then atropisomerism [42–44] which is defined to occur when the barrier is larger than 22 kcal mol^{-1}. This rotational barrier in MC has been determined experimentally to be $E_a = 36.9 \pm 3$ kcal mol^{-1} (isomerization half-lives of 50.6 h at 128 °C and 3 h at 154 °C) [44], while we

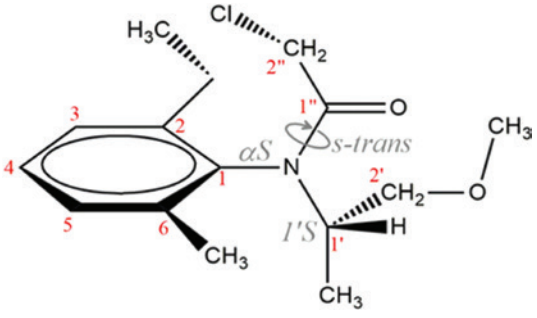

Fig. 1: Structure of S-metolachlor, indicating the elements of symmetry.

calculated it as 34.9 kcal mol^{-1} in our former work [37]. The phenyl and amidyl planes adopt an almost perpendicular position. The C–Cl bond suffers scission under photolytic conditions, giving rise to the radical species without chlorine (which we called MCRad), with the unpaired electron localized on the amidyl residue. Stable conformers of MC and MCRad were characterized in [37].

Geometry optimizations in this work were performed using density functional theory (DFT) [45]. There are numerous methods that can be chosen for this task. The Minnesota functional M06 [46] is one of the modern versions, which presents a reasonable balance between accuracy and resources required, something important for relatively large molecules as the ones studied here. M06 is a hybrid meta-generalized gradient-approximation DFT method, including not only the density and its gradient, but also the kinetic energy density. A set of parameters in the method were adjusted in the original publication using a high quality benchmark database. The comparison in that paper with the results obtained using other 12 different functionals showed that M06 has a very good behavior for the description of a combination of main-group thermochemistry, kinetics, and non-covalent interactions. To that end, it was once more the method chosen in this study.

Although DFT methods do not have a large dependence on the basis set, as molecular orbital methods have, the choice of a reasonably complete set is nonetheless important to obtain good results. Due to the large size of the molecules studied, a relatively small 6-31 + G(d,p) basis set was employed for the exploration steps. A larger basis set, namely Dunning's correlation consistent cc-pVTZ, was used to refine the calculations. Geometry optimizations were performed with a threshold of 10^{-4} Å in all interatomic distances, and an ultrafine grid was used to perform numerical integrations. Second derivatives of the energy with respect to the nuclear coordinates were calculated analytically both to characterize the critical points on the PES and to obtain thermochemical properties.

Reaction enthalpies, $\Delta_r H^o$, and free energies, $\Delta_r G^o$, at 298.15 K in gas phase, have been obtained using the rigid rotor, harmonic oscillator approximation by standard formulas of statistical thermochemistry. To assess the accuracy of the results, these values were additionally calculated using the CBS-QB3 methodology [47] which besides optimization of the geometries at the DFT level, includes corrections for extension of the basis set and more precise dynamical correlation. This method provides an approximation to the more complete (and unfeasible for molecules of this size) CCSD(T)/CBS procedure.

It has been shown that a more complete consideration of the conformation of molecules in aqueous solution and their corresponding vibrational spectra are in many cases improved by taking into account specific interactions between the solute and solvent molecules. To that end, the bulk effect of the solvent in aqueous solution was simulated using the polarizable continuum model (PCM) with standard parameters [48].

All calculations were performed with the G09 suite of computer codes [49].

Results and discussion

The main results obtained in this work are the structure and energetics of the reactants, intermediates, transition states and products of the hydoxylation products. The general scheme of the reactions, according to our calculations, is shown in Fig. 2. Only the most stable isomers of MC and MCRads, obtained in our previous study [37], were used in this work.

It is generally admitted that the photo oxidation of MC under environmental conditions starts with Cl elimination by photocatalytic cleavage of the C–Cl bond, leading to the formation of MCrad [26, 27, 29, 30]. We calculated the binding energy of the C–Cl bond as 74.1 kcal mol^{-1} at the M06/6-31 + G(d,p) level of theory in our former work [37]. A better estimation done in this paper at the M06/cc-pVTZ level affords a value of 74.7 kcal mol^{-1}, showing that the basis set in this case is not a critical issue (structures of all the species are shown in Figs. 3, for the minima, and 4, for the transition states; detailed information on their geometries can be obtained directly from the authors).

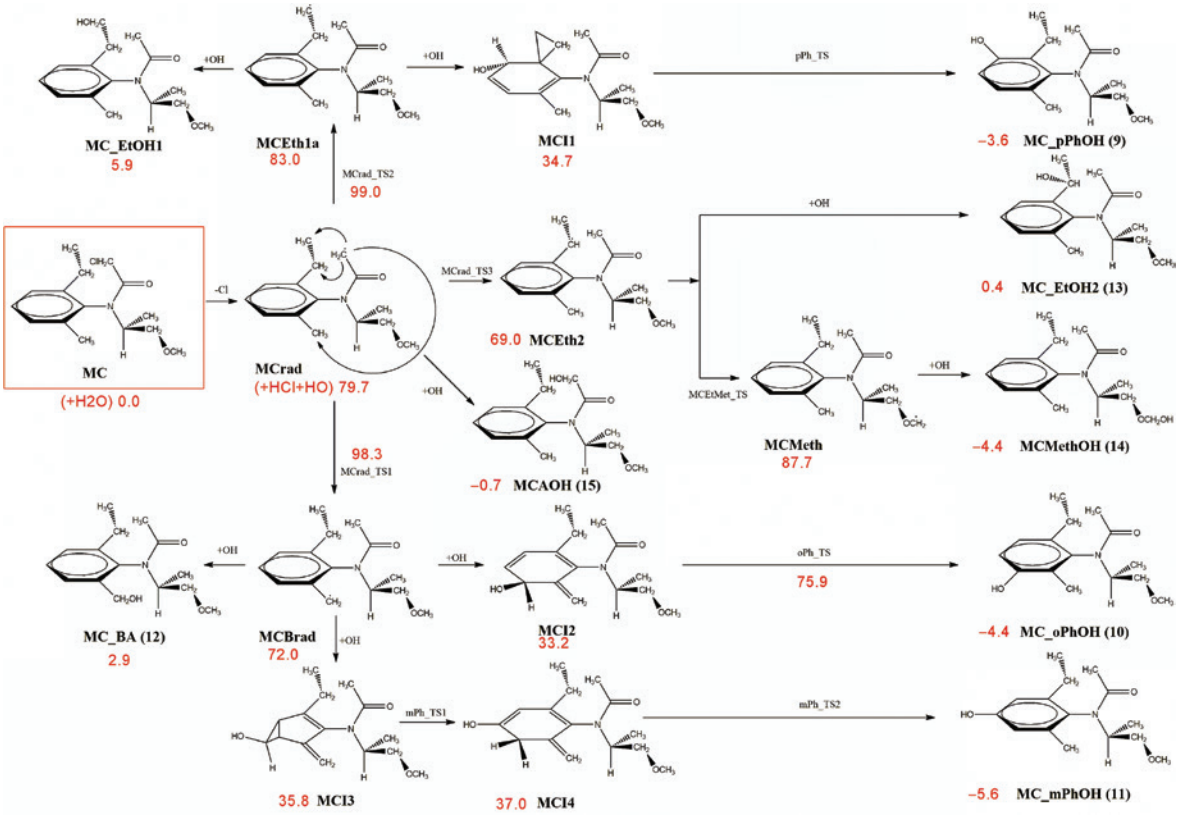

Fig. 2: Schematic diagram of the main processes in the photodegradation of MC in the presence of OH radicals.

Experimentally, most of the products of the photodegradation process are hydroxylated species, as shown in a detailed study by Bouchonnet et al. [27, 29] under simulated sunlight conditions, although cyclization products and morpholinone derivatives have also been mentioned in other reports [28]. Notice that this hydroxylated products do not come from reaction of the hydroxyl radical with the unreacted MC molecule, but from different transformations of the dechlorinated species MCRad. As said in the introduction, under different environmental conditions hydroxylation of MC may be the preferred channel, but this was not the focus of this study.

The initial step of the different mechanisms, once the MCrad species is formed, is an internal hydrogen transfer. Notice that, in principle, the OH radical could react with the amidyl radical directly (i.e. without previous H-transfer) to give MCAOH in the scheme of Fig. 2. This species is numbered as **15** in the work of Coffinet et al. [29]. However, the relative abundance of this isomer is just 1.1 %. A possible explanation of this behavior will be discussed later.

Three radicals can be obtained by hydrogen abstraction from positions *1* or *2* of the ethyl, or from the methyl substituents on the phenyl ring. We have labelled them as MCrad1, MCrad2 and MCrad3, respectively in Fig. 2. They give rise to several products which have been labelled using the same numbers as in the paper by Coffinet et al. [29].

In our previous work [37] we have determined the abundance order to be **11** > **10** ≃ **14** > **9** > **15** > **13** > **12**, based solely on the thermochemical stability of the products with the use of the M06/6-31+G(d,p) $\Delta_r G^0_{298}$ values, while at the CBS level we have obtained **14** > **10** > **9** > **11** > **13** > **15** ≫ **12**. The experimental determination followed the order **9** > **10** > **11** ≫ **12** ≫ **14** > **13** ≃ **15**. Therefore, just based on the enthalpies of formation the order is not only wrong, no matter the level of theory, but also **14** appears to be very stable, while it is barely observable experimentally, and **12** comes out to be the least stable, while experimentally it is observed with a small but noticeable 6.2 % abundance [29]. These were the discrepancies that we settled down to resolve in this work, calculating the reaction paths that lead to the observed major and minor products.

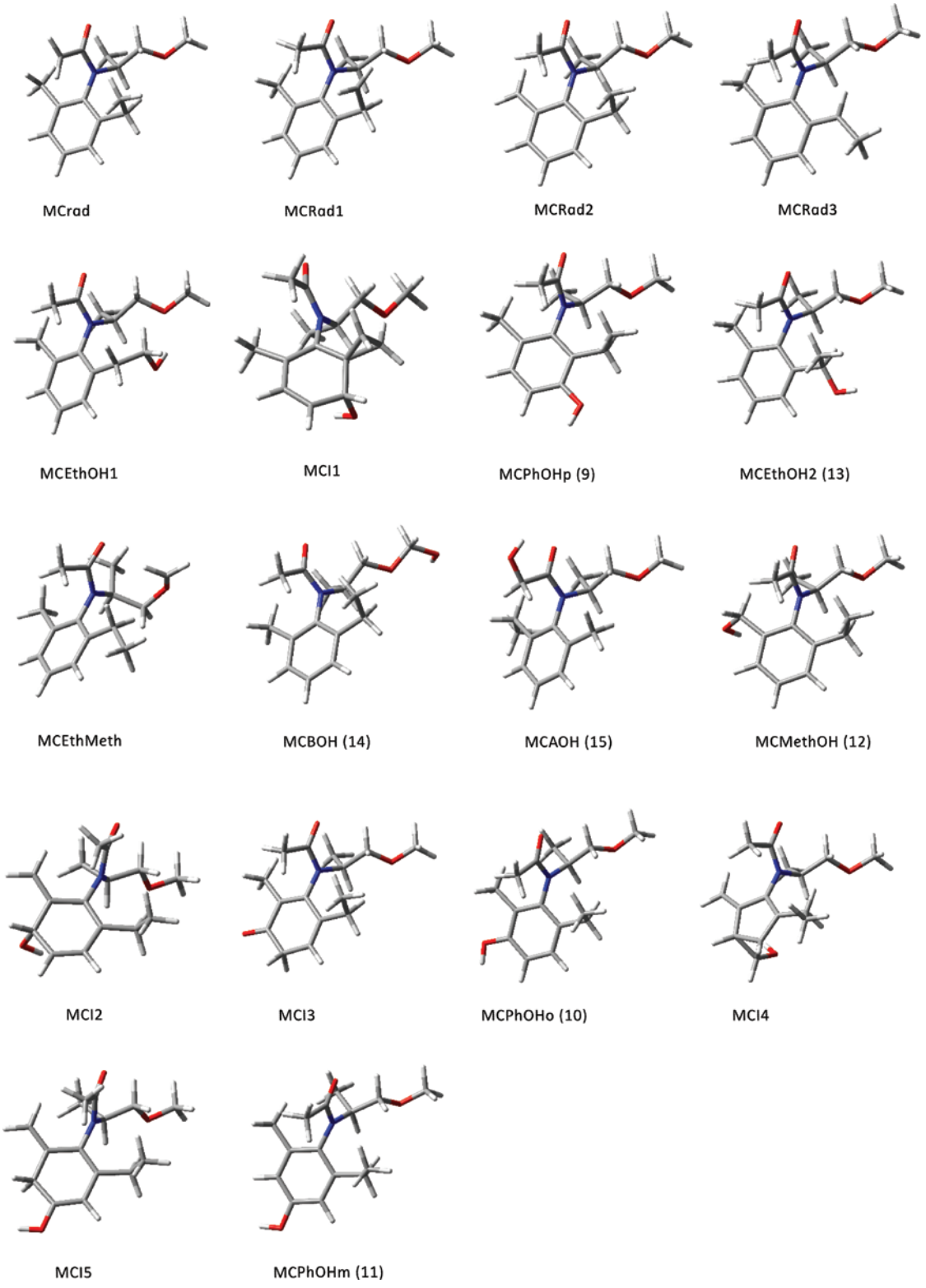

Fig. 3: Optimized structures of the reactants, intermediates and products indicated in the scheme of Fig. 2.

The initial diagram we will discuss is presented in Fig. 5, which shows the relative energies (including ZPE) at the M06/6-31+G(d) level, of the reactants, intermediates, transition states and products with respect to MCrad + OH + HCl (we assumed that the initial formal reaction was MC + H_2O to maintain mass balance) in

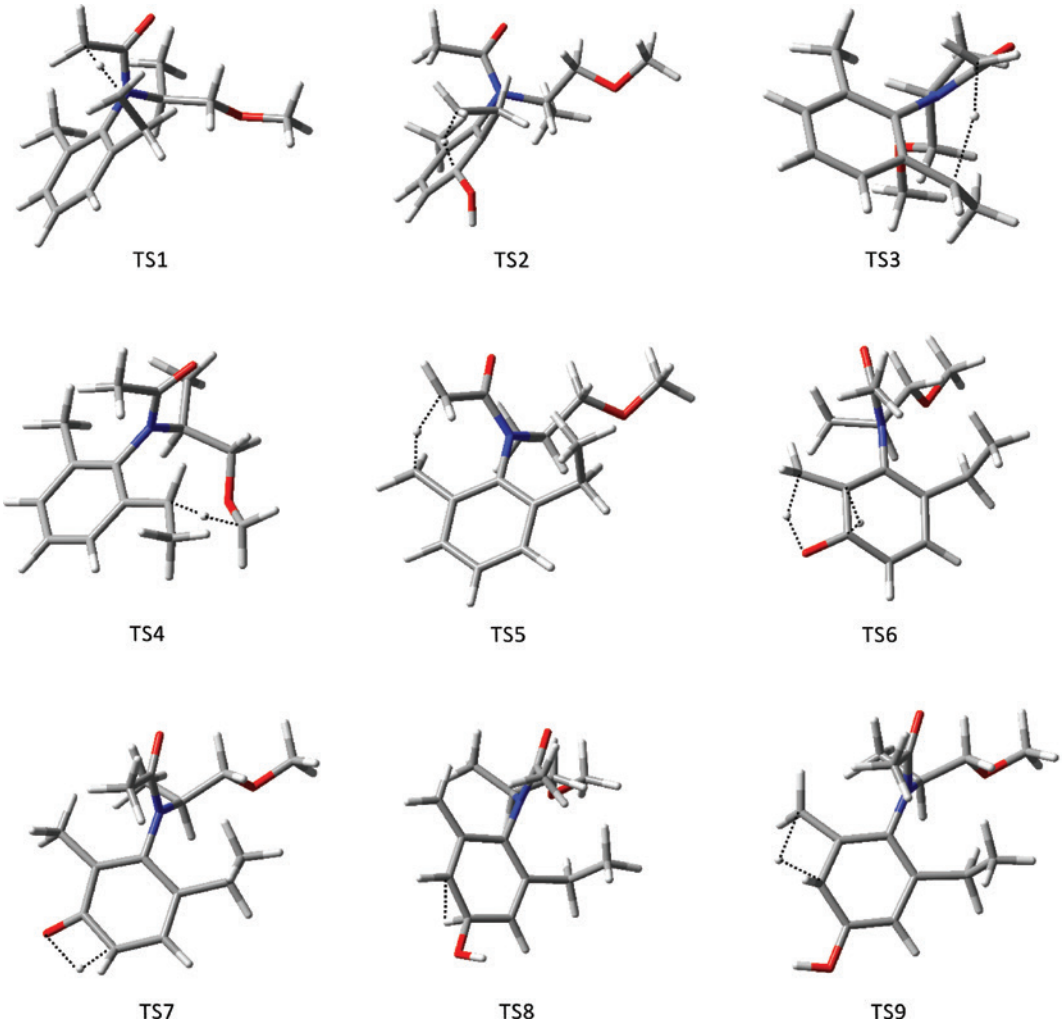

Fig. 4: Structure of the transition states in the paths from reactants to products, according to the nomenclature included in the scheme of Fig. 2.

gas phase. For this initial discussion we have assumed that the reactions between MCrad1-MCrad3 with the OH radical occur without barriers, while the intermediates formed, MCI1 to MCI4 are separated from the final products by one or more transition states.

The first question that poses itself immediately is why the reaction paths going through TS1, TS5 and TS3 toward MCrad1, MCrad2 andMCrad3 would be preferred, instead of the more direct reaction of MCrad with OH to give **15**. Species **15** could be difficult to obtain either because MCrad transforms very fast to MCrad1-MCrad3 or because of some kind of sterical impediment which prevents the OH from reaching the radical center. The first hypothesis is contradicted by the height of the barriers, large enough to require a substantial time for the hydrogen transfer. Notice that the addition of the solvent would not help these processes by any way of catalysis, since the radical center and the hydrogens to be abstracted are very near. Tunneling effects, which we did not calculate in this paper, might be important but not to that extent. The sterical impediment explanation, on the other side, carries more weight. Presented in Fig. 6 is the vdW model of MCrad, showing specifically the surroundings of the radical center. It can be noticed that both sides of the planar radical are reasonably protected from outside interaction by the alkyl substituents of the phenyl ring. Thus, internal H-transfer is more likely to occur than the interaction with an external OH radical and product **15** will be obtained in low yields, as actually observed in the experiment. Notice that even if an OH radical would try to approach the CH_2 radical center, it would encounter first either other labile hydrogens or the aromatic ring, causing therefore other reactions than that conducting to product **15**.

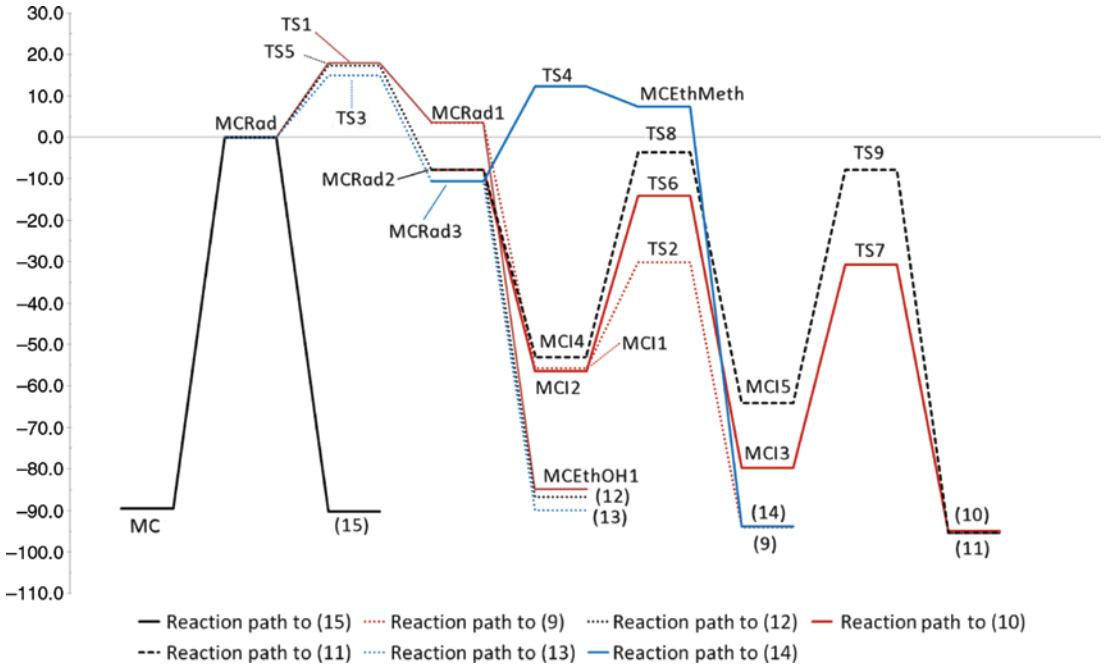

Fig. 5: Relative energies (E + ZPE) in gas phase of the different reactants, intermediates, transition states and products with respect to MCRad + HCl + OH, in kcal mol^{-1}.

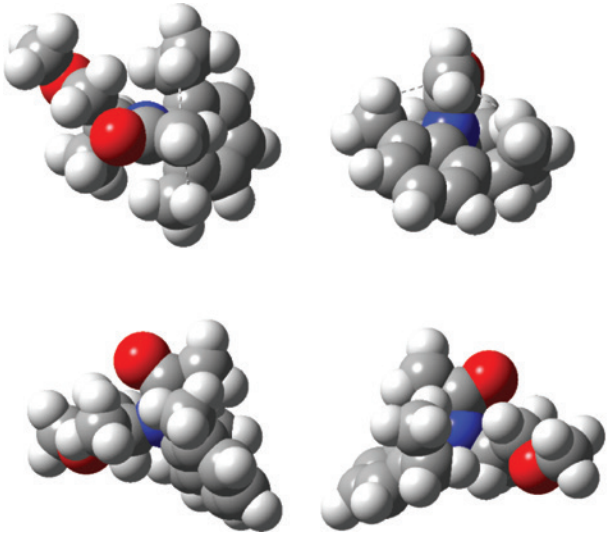

Fig. 6: Upper, front, right- and left-side views of the vdW model of the MCRad species, showing the protective role of the alkyl substituents on the ring toward the amidyl CH_2 radical.

The transition state TS1, which leads to MCRad1 with the radical center now at the far end of the ethyl substituent, is the least stable out of the three TS1, TS3, TS5. Although the barriers are very similar (17.9, 15.0 and 17.4 kcal mol^{-1}, respectively at the M06/6-31 + G(d,p) level and 17.7, 15.5 and 17.7 kcal mol^{-1} at the M06/cc-pVTZ level), TS1 is not only the largest one, but also leads to the least stable H-transfer radical, MCRad1 (all energies for the species at the different levels of calculation used in this paper are shown in Table 1, notice that the CBS-QB3 value for TS1 is also in agreement with the DFT calculations). Two paths are now open. On the one side, direct reaction of the OH radical at the ethyl $-CH_2CH_2$ radical center would lead to MCEthOH1, with a terminal alcohol group which nonetheless is not observed at all experimentally.

Table 1: Total electronic energy E_t + ZPE (in Hartrees) and relative energies (in kcal mol^{-1}) for the different species studied in this work.

Species[a]	M06						CBS-QB3	
	6-31+G(d,p)				cc-pVTZ			
	E_t+ZPE[b]	Δ(E_t+ZPE)[b]	*E_t+ZPE*[c]	*Δ(E_t+ZPE)*[c]	E_t+ZPE[b]	Δ(E_t+ZPE)[b]	E_t+ZPE[b]	Δ(E_t+ZPE)[b]
HCl	−460.75879		*−460.762475*		−460.81453		−460.35483	
OH	−75.69253		*−75.698121*		−75.72983		−75.65806	
H_2O	−76.37616		*−76.384791*		−76.37616		−76.35859	
MC + H_2O	−1325.74169	−89.5	*−1325.761275*	*−90.2*	−1326.01834	−77.4	−1324.711370	−93.8
MCRad + HCl + OH	**−1325.59905**	**0.0**	***−1325.617554***	***0.0***	**−1325.89493**	**0.0**	**−1324.56195**	**0.0**
TS1 + HCl + OH	−1325.57057	17.9	*−1325.591258*	*16.5*	−1325.86673	17.7	−1324.53491	17.0
MCRad1 + HCl + OH	−1325.59342	3.5	*−1325.613887*	*2.3*	−1325.89001	3.1	−1324.90808	3.5
MCEthOH1 + HCl	−1325.73427	−84.8	*−1325.751914*	*−84.3*	−1326.01337	−74.3	−1324.702330	−88.1
MCI1 + HCl	−1325.68794	−55.8	*−1325.706352*	*−55.7*	−1325.96655	−44.9	−1324.65062	−55.6
TS2 + HCl	−1325.64716	−30.2	*−1325.640659*	*−31.0*	−1325.92230	−17.2	−1324.590750	−18.1
MCPhOHp (9) + HCl	−1325.74882	−94.0	*−1325.766659*	*−93.6*	−1326.02992	−84.7	−1325.07829	−96.6
MCAOH (15) + HCl	−1325.74283	−90.2	*−1325.758437*	*−88.4*	−1326.02144	−79.4	−1325.07366	−92.8
TS5 + HCl + OH	−1325.57140	17.4	*−1325.591411*	*16.4*	−1325.86673	17.7	−1324.549865	7.6
MCRad2 + HCl + OH	−1325.61161	−7.9	*−1325.631527*	*−8.8*	−1325.90810	−8.3	−1324.574410	−7.8
MCMethOH (12) + HCl	−1325.73728	−86.7	*−1325.75487*	*−86.2*	−1326.01653	−76.3	−1325.06829	−89.5
MCI2 + HCl	−1325.68911	−56.5	*−1325.707466*	*−56.4*	−1325.96813	−45.9	−1324.664535	−64.4
TS6 + HCl	−1325.62151	−14.1	*−1325.645769*	*−17.7*	−1325.89027	2.9	−1324.582739	−13.0
MCI3 + HCl	−1325.72611	−79.7	*−1325.746412*	*−80.9*	−1326.00571	−69.5	−1324.695364	−83.7
TS7 + HCl	−1325.64794	−30.7	*−1325.665443*	*−30.1*	−1325.92733	−20.3	−1324.612785	−31.9
MCPhOHo (10) + HCl	−1325.75038	−95.0	*−1325.768235*	*−94.6*	−1326.03030	−84.9	−1325.07980	−97.4
MCI4 + HCl	−1325.68270	−52.5	*−1325.700565*	*−52.1*	−1325.96184	−42.0	−1324.65033	−55.5
TS8 + HCl	−1325.60497	−3.7	*−1325.608948*	*−5.4*	−1325.88487	6.3	−1324.581282	−12.1
MCI5 + HCl	−1325.70118	−64.1	*−1325.72013*	*−64.4*	−1325.98188	−54.6	−1324.672385	−69.3
TS9 + HCl	−1325.61161	−7.9	*−1325.630092*	*−7.9*	−1325.89130	2.3	−1324.57798	−10.1
MCPhOHm (11) + HCl	−1325.75108	−95.4	*−1325.76983*	*−95.6*	−1326.03054	−85.1	−1325.07859	−96.8
TS3 + HCl + OH	−1325.57515	15.0	*−1325.595207*	*14.0*	−1325.87019	15.5	−1324.553547	5.3
MCRad3 + HCl + OH	−1325.61605	−10.7	*−1325.63618*	*−11.7*	−1325.91219	−10.8	−1324.592625	−19.2
MCEthOH2 (13) + HCl	−1325.74236	−89.9	*−1325.760685*	*−89.8*	−1325.02163	−79.5	−1325.07346	−93.4
TS4 + HCl + OH	−1325.57950	12.3	*−1325.59929*	*11.5*	−1325.87397	13.2	−1324.555685	3.9
MCEthMeth + HCl + OH	−1325.58732	7.4	*−1325.614567*	*1.9*	−1325.88343	7.2	−1324.573779	−7.4
MCBOH (14) + HCl	−1325.74861	−93.8	*−1325.767088*	*−93.8*	−1326.02726	−83.0	−1325.08006	−97.0

[a]The product species have been identified with the same numbers used in the work by Coffinet et al. [29]; [b]Gas phase; [c]PCM simulated solvent. Relative energies are expressed with respect to MCRad + HCl + OH at each of the levels of calculation used. The numbers in bold represent the reference with respect to which the other relative energies are calculated. The numbers in italic represent the results in solvation.

In contrast, the OH radical could add to the *para* position at the ring (because of congruence with our studies on toluene, we would adopt the unconventional nomenclature of *ortho*, *meta* and *para* **with respect to the methyl group on the ring**). If this happens, then the terminal CH_2 radical also attacks the ring and forms a three membered additional ring that forms the spiran structure MCI1 which, by a simple H-transfer from the benzene ring to the cyclopropane ring ends up giving structure **9**.

The process described in the former paragraph hints to a possible failure in our reasoning. If there were no barriers for the reaction of the MCRad1 and OH radicals, then MCEthOH1 should be observed experimentally, but it is not. We will look further into this problem later on.

The second transition state in energy is TS5 which leads to MCRad2, where the unpaired electron is located on the former CH_3 substituent of the aromatic ring, after H-transfer to the amidyl radical (see Fig. 7). Three paths are now open for further reactions. One of them is the direct reaction of OH with the CH_2 radical center which would lead to the alcohol **12**. This is a possible but not favored path, because resonance with the ring makes a very stable delocalized radical. Breaking this delocalization at one of the possible sites of the ring leads to the intermediates MCI2 and MCI4 which further evolve to **10** and **11**, but with barriers that are not present for the obtainment of **12**. This process is similar to what happens in the reaction of the benzyl radical, derived from toluene, with the OH radical, where the main observed products are cresols and benzaldehyde, but not benzyl alcohol except in special cases.

MCI2 is actually very close in energy to MCI1, but while the latter leads to **9** traversing only one transition state (TS2), MCI2 goes first to a quinonic intermediate through a transition state with a larger barrier than MCI1. In fact, the TS6-MCI2 barrier is 42.4 and 48.9 kcal mol^{-1} at the two DFT levels of theory we are using, while it is only 25.6 and 27.8 kcal mol^{-1} for TS2-MCI1. Therefore, depending on the concentration of the MCI1 and MCI2 intermediates, formation of **9** should be more favorable than formation of **10**, in agreement to experiment, even if the enthalpy of reaction is slightly more negative for **10**.

MCI4 is less stable than MCI2, exhibiting a fused ring structure which, through the TS8 and TS9 transition states allows for hydrogen migration paths ending up to **11.** The transition states TS8 and TS9 are less stable than TS6 and TS7, and both TS8 and TS6 are less stable than TS2, which implies that **11** will be obtained in less abundance than **10** or **9**, exactly as is observed experimentally.

Finally, the most stable H-transfer radical MCRad3, where the radical center is located at the secondary carbon of the ethyl substituent (see Fig. 7), is reached through the also more stable transition state TS3. As in the other cases, two products can be reached; **13** by a direct reaction of the two radicals MCRad3 and OH, or **14** through a transition state TS4 and an intermediate MCEthMeth. While we will talk about the direct addition later, it is worth mentioning now that even if the reaction enthalpy of **14** is similar to that of **9**, **10** and **11**, TS4 is much higher in energy than any of the other transition states. This explains then why **14** is observed experimentally in small amounts, while it would not be so if relying only on the enthalpies of formation.

To solve completely the puzzle of the discrepancies between our former study and the experimental results, we must explain why **12** and **13** are observed in small amounts and MCEthOH1 not observed at all in the experiments, even if direct reaction with OH at the radical centers would lead to very favorable energy drops,

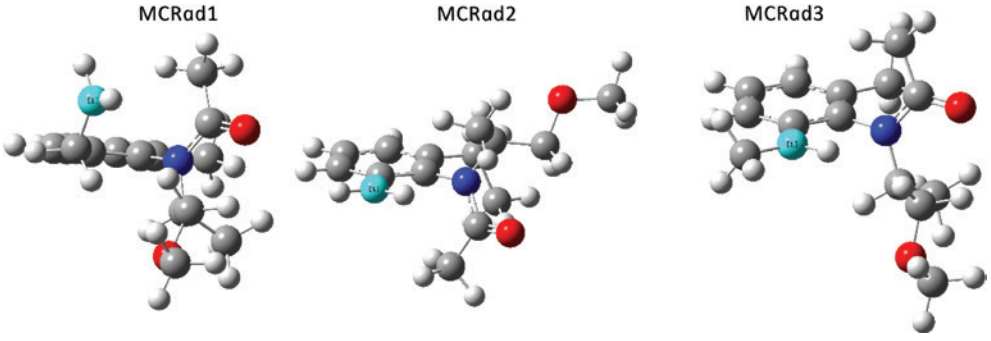

Fig. 7: Structure of the three intermediate H-transfer radicals MCRad1, MCRad2 and MCRad3. The carbon bearing the unpaired electron is color-coded light blue and bears the number [1].

making the products almost as stable as the observed ones **9**, **10** and **11**. The only possible explanation is that our initial assumption that there is no transition state for the addition of OH at the radical center is wrong.

In the case of **12**, that would arise from the direct reaction of OH with the methylene radical center formed from the CH_3 substituent in the aromatic ring, the explanation is relatively easy. Looking at the structure of MCRad2, the precursor of **12** (see Fig. 5), it is noticeable that the CH_2 radical center is delocalized with the ring and somehow stacked (although not completely) between two methyl residues on the amidyl group. These would tend to disfavor the interaction of the OH radical with the CH_2 group and to redirect the reaction toward addition to the ring, a similar phenomenon to that noticed in toluene. In a certain sense, the difficulty in attacking the benzyl radical at the CH_2 center is analogous to what we described for the amidyl radical (see Fig. 4). Therefore, nothing remains unexplained in this case.

13 is a similar case. The radical center on the CH group is delocalized and therefore exhibits the same preference for OH to add to the ring instead of this carbon. Notice that the radical center is not so well protected in MCRad3 as it is in MCRad2 by the substituents in the amidyl residue, but the methyl group on the radical center contributes to the shielding environment. Thus, the explanation for the small abundance of **13** would be analogous to that given for **12**.

However, the complete absence of MCEthOH1 from the experimentally observed products is puzzling. Since it is the least stable of all the products, it might well be that it would be present in a small amount, but its complete absence is a problem in itself (of course, keeping in mind that perhaps it could not be experimentally identified even if it was present). The structure of MCRad1, the putative precursor of MCEthOH1, is shown also in Fig. 5. It can be seen that there is neither a steric impediment for the approach of the OH radical nor a stabilization by delocalization of the CH_2 radical center. Therefore, our calculations predict that MCEthOH1 should be obtained is small quantities, certainly less than **13**, **14** and **15**, but should nonetheless be observable.

A further analysis concerns the relative abundance of compounds **9**–**12**, which we have found as the most relevant species. According to the preceding discussion, once the intermediates MCI1, MCI2 and MCI4 (which have quite similar energies) are formed, kinetics favor **9**, **10** and **11**, in that order. The transition states for acquiring the three principal isomers of MCRad (MCRad1, MCRad2 and MCRad3) also have quite similar energies, although MCRad1 (the precursor of **9**) is a less stable intermediate than the other two. The equilibrium should then be shifted toward MCRad2 (the precursor of **10**, **11** and **12**) and MCRad3, the precursor of **13** and **14**. Most of MCRad3 will not react and end up being redistributed between MCRad1 and MCRad2, which will evolve to MC1, MC2 and MC4. While all the concentration of MCRad1 goes into MCI1, that of MCRad2 will be divided into MCI2 and MCI4. MCI4 will then proceed with the higher barriers toward **11**, while MCI1 will evolve to **9** and MCI2 to **10**. Given now the height of the barriers involved, **9** will appear much faster than **10**. Putting now all these data together, the order of abundances should be $\mathbf{9} > \mathbf{10} > \mathbf{11} \gg \mathbf{12} \simeq \mathbf{13} > \mathbf{14} \simeq \mathbf{15}$ which is very similar to the experimental one, although our calculations do not allow to determine precisely the order of **12** and **13**, and of **14** and **15**, which nonetheless are minor products.

Finally, one could ask whether the presence or absence of the water solvent affects the calculations. We have included in this study the effect of bulk water, using a self-consistent reaction field (SCRF) approach, specifically Tomasi et al. Polarizable Continuum Model [48]. No microsolvation was attempted, which may be the subject of further work. Comparing the results shown in Table 1 at the 6-31+G(d,p) level, it is clear that there is no qualitative difference in the discussion, even if some small quantitative effect is noticed. The conclusion is that if any solvent effect is observed, it is not due to bulk polarization by the solvent but, if at all, by the presence of one or two auxiliary water molecules which may move barriers downwards, as it is known to occur in other reactions (see, for instance, ref. [50]).

Conclusions

A detailed computational chemistry analysis of the reaction paths leading to the major mono-hydroxylated products of the photofragmentation product of metolachlor, after the attack of a hydroxyl radical has been performed. The structures of reactants, intermediates, transition states and products were determined

resorting to DFT calculations using the M06 exchange-correlation functional and medium and large size basis sets, as well as the *ab initio* composite CBS-QB3 method.

The results indicate that a combination of thermodynamic and kinetic factors do explain the relative abundance of the products observed experimentally. Product **14**, that in our previous work was competing with the major products, but was not observed in such an abundance experimentally, was shown to be scarce because of the much higher transition state TS4, with respect to the other paths. Products **12** and **13** were shown to be less favorable than **9**, **10** and **11** because the precursors exhibit a strong delocalization of the radical with the aromatic ring and a protective effect of the alkyl substituents on the amidyl residue. Addition to the ring is then strongly favored against direct addition to the radical center. While radical-radical reactions normally exhibit no intrinsic barrier [36, 51], diffusion or steric related factors may favor one type of addition over another, as it happens in these cases.

The three internal H-transfer intermediates MCRad1, MCRad2 and MCRad3 exhibit the expected behavior. MCRad1, with the radical centered at the distal CH_3 group in the ethyl substituent of the ring, is the least stable, followed by the species with the radical centered at the methyl substituent, MCRad2, and with MCRad3, the species where the radical center is at the secondary carbon of the ethyl group, the most stable one. The intermediates obtained from them by addition of the OH, MCI1, MCI2 and MCI4, are however very near in energy. From these intermediates, species **9** is obtained more easily, justifying its prevalent abundance, followed by **10** and then **11**, in agreement to the observed facts.

Our calculations did not allow us to explain why the compound MCEthOH1, arising also from the MCrad1 intermediate, is not observed albeit at a small concentration. Its stabilization energy obtained with the theoretical methods used is the smallest of all the products, implying then a small abundance, but there is no theoretically discernible reason for which it must be completely absent. More experimental work seems in order to try to find this isomer.

Our study shows that the M06 method is reasonably accurate for the prediction of possible reaction paths occurring from the addition of OH to the intermediate H-transfer radicals. Therefore, the conclusions provided here could be used with confidence in order to study further experimentally the different reaction products observed.

References

[1] J. N. Aubertot, J. M. Barbier, A. Carpentier, J. N. Gril, L. Guichard, P. Lucas, S. Savary, M. Voltz. *Pesticides, agriculture et environnement. Réduire l' utilisation des pesticides et en limiter les impacts environnementaux. Rapport d'Expertise scientifique collective Inra-Cemagref* [*Pesticides, agriculture and environment: To reduce the use of pesticides and limit the environmental impacts. Report of collective expertise Inra-Cemagref*] (2005).
[2] J. E. Barbash, G. P. Thelin, D. W. Kolpin, R. Gilliom. *Distribution of major herbicides in ground water of the United States*. U.S. Geological Survey, Water-Resources Investigations, Report 98-4245, Sacramento, CA (1999).
[3] D. S. Aga, S. Heberle, D. Rentsch, R. Hany, S. R. Müller. *Environ. Sci. Technol.* **33**, 3462 (1999).
[4] G. Chesters, G. V. Simsiman, J. Levy, B. I. Alhajjar, N. Riyadh, R. N. Fathulla, J. M. Harkin. *Rev. Environ. Contamin. Toxicol.* **110**, 1 (1989).
[5] H. Y. F. Ng, J. D. Gaynor, C. S. Tan, C. F. Drury. *Water Res.* **29**. 2309 (1995).
[6] R. Mathew, S. U. Khan. *J. Agric. Food Chem.* **44**, 3996 (1996).
[7] P. J. O'Connell, C. T. Harms, J. R. F. Allen. *Crop Protection* **17**, 207 (1998).
[8] L. Fava, P. Bottoni, A. Crobe, E. Funari. *Chemos.* **41**, 1503 (2000).
[9] S. M. Novak, J. M. Portal, M. Schiavon. *Chemos*. **42**, 235 (2001).
[10] C. Accinelli, G. Dinelli, A. Vicari. *Biol. Fertile Soils* **33**, 495 (2001).
[11] D. Sanyal, G. Kulshrestha. *J. Agric. Food Chem.* **50**, 499 (2002).
[12] P. A. Rice, T. A. Anderson, J. R. Coats. *Environ. Toxic. Chem.* **21**, 2640 (2002).
[13] W. Mersie, C. McNamee, C. Seybold, J. Wu, D. Tierney. *Environ. Toxic. Chem.* **23**, 2627 (2004).
[14] A. B. Caracciolo, G. Giuliano, P. Grenni, L. Guzzella, F. Pozzoni, P. Bottoni, L. Fava, A. Crobe, M. Orru, E, Funari. *Environ. Poll.* **134**, 525 (2005).
[15] Z. Vryzas, E. N. Papadakis, K. Oriakli, T. P. Moysiadis, E. Papadopoulou-Mourkidou. *Chemos.* **89**, 1330 (2012).

[16] J. H. Prueger, J. Alfieri, T. J. Gish, W. P. Kustas, C. S. T. Daughtry, J. L. Hatfield, L. G. McKee. *Water Air Soil Pollut.* **228**, 84 (2017).
[17] J. Kochany, J. R. Maguire. *J. Agric. Food Chem.* **42**, 406 (1994).
[18] J. J. Pignatello, Y. Sun. *Wat. Res.* **29**, 1837 (1995).
[19] Y. J. Lin, M. Karuppiah, A. Shaw, G. Gupta. *Ecot. Environ. Saf.* **43**, 35 (1999).
[20] R. I. Wilson, S. A. Mabury. *J. Agric. Food Chem.* **48**, 944 (2000).
[21] G. Dinelli, C. Accinelli, A. Vicari, P. Catizone. *J. Agric. Food. Chem.* **48**, 3037 (2000).
[22] V. A. Sakkas, I. M. Arabatzis, I. K. Konstantinou, A. D. Dimou, T. A. Albanis, P. Falaras. *App. Cat. B: Environ.* **49**, 195 (2004).
[23] A. D. Dimou, V. A. Sakkas, E. A. Albanis. *J. Agric. Food. Chem.* **53**, 694 (2005).
[24] M. L. Hladik, E. J. Bouwer, A. L. Roberts. *Water. Res.* **42**, 4905 (2008).
[25] P. M. White, Jr, T. L. Potter. *J. Environ. Sci. Health B* **45**, 728 (2010).
[26] P. H. Goulden, S. Coffinet, C. Genty, S. Bourcier, M. Sablier, S. Bouchonnet. *Anal. Chem.* **83**, 7587 (2011).
[27] S. Bouchonnet, S. Kinani, Y. Souissi, S. Bourcier, M. Sablier, P. Roche, V. Boireau, V. Ingrand. *Rapid Commun. Mass Spectrom.* **25**, 93 (2011).
[28] J. Restivo, J. J. M. Orfao, S. Armenise, E. Garcia-Bordeje, M. F. R. Pereira. *J. Hazard Mat.* **239–240**, 249 (2012).
[29] S. Coffinet, A. Rifai, C. Genty, Y. Souissi, S. Bourcier, M. Sablier, S. Bouchonnet. *J. Mass Spectrom.* **47**, 1582 (2012).
[30] Y. Souissi, S. Bouchonnet, S. Bourcier, K. O. Kusk, M. S. Henrik, R. Andersen. *Sci. Total Environ.* **458–460**, 527 (2013).
[31] R. Otero, D. Esquivel, M. A. Ulibarri, F. J. Romero-Salguero, P. Van der Voort, J. M. Fernandez. *Chem. Eng. J.* **251**, 92 (2014).
[32] E. Nicol, C. Genty, S. Bouchonnet, S. Bourcier. *Rapid Commun. Mass Spectrom*. **29**, 2279 (2015).
[33] C. A. Orge, M. F. R. Pereira, J. L. Faria. *Chem. Eng. J.* **318**, 247 (2017).
[34] J. Hoigné, F. Morel. "The Kinetics of Trace Metal Complexation: Implications for Metal Reactivity in Natural Waters", in *Aquatic Chemical Kinetics: Reaction Rates of Processes in Natural Waters*, W. Stumm (Ed.), p. 560, Wiley, New York (1990).
[35] J. Mack, J. R. Bolton. *J. Photochem. Photobiol. A* **128**, 1 (1999).
[36] S. Gligorovski, R. Strekowski, S. Barbati, S. Vione. *Chem. Rev.* **115**, 13051 (2015).
[37] Z. Salta, A. M. Kosmas, O. N. Ventura. *Theoret. Chem. Acc.* **137**, 151 (2018).
[38] H. U. Blaser. *Adv. Syn. Catal.* **344**, 17 (2002).
[39] A. Kant Kabler, S. Chen. *J. Agric. Food. Chem.* **54**, 6153 (2006).
[40] C. Klein, R. J. Schneider, M. T. Meyer, D. S. Aga. *Chemos.* **62**, 1591 (2006).
[41] M. Y. Z. Aboul Eish, M. J. M. Wells. *J. Chromat. Sci.* **46**, 269 (2008).
[42] O. Machinori, "Recent advances in atropomerism", in *Topics in stereochemistry*, N. L. Allinger, E. L. Eliel, S. H. Wilen (Eds.), Hoboken, John Wiley (1983).
[43] I. Alkorta, J. Elguero, C. Roussel, N. Vanthuyne, P. Patrick Piras. *Adv. Heterocyc. Chem.* **105**, 1 (2012).
[44] H. Moser, G. Rihs, H. Sauter. *Z. Naturforsch.* **37b**, 451 (1982).
[45] W. Koch, M. C. Holthausen. *A Chemist's Guide to Density Functional Theory*, Wiley VCH Verlag GmbH, Heidelberg, Germany (2001).
[46] Y. Zhao, D. G. Truhlar. *Theor. Chem. Acc.* **120**, 215 (2006).
[47] J. A. Montgomery Jr., M. J. Frisch, J. W. Ochterski, G. A. Petersson. *J. Chem. Phys.* **112**, 6532 (2000).
[48] J. Tomasi, B. Mennucci, R. Cammi. *Chem. Rev.* **105**, 2999 (2005).
[49] Gaussian 09, Revision D.01, M. J. Frisch, G. W. Trucks, H. B. Schlegel, G. E. Scuseria, M. A. Robb, J. R. Cheeseman, G. Scalmani, V. Barone, B. Mennucci, G. A. Petersson, H. Nakatsuji, M. Caricato, X. Li, H. P. Hratchian, A. F. Izmaylov, J. Bloino, G. Zheng, J. L. Sonnenberg, M. Hada, M. Ehara, K. Toyota, R. Fukuda, J. Hasegawa, M. Ishida, T. Nakajima, Y. Honda, O. Kitao, H. Nakai, T. Vreven, J. A. Montgomery Jr., J. E. Peralta, F. Ogliaro, M. Bearpark, J. J. Heyd, E. Brothers, K. N. Kudin, V. N. Staroverov, T. Keith, R. Kobayashi, J. Normand, K. Raghavachari, A. Rendell, J. C. Burant, S. S. Iyengar, J. Tomasi, M. Cossi, N. Rega, J. M. Millam, M. Klene, J. E. Knox, J. B. Cross, V. Bakken, C. Adamo, J. Jaramillo, R. Gomperts, R. E. Stratmann, O. Yazyev, A. J. Austin, R. Cammi, C. Pomelli, J. W. Ochterski, R. L. Martin, K. Morokuma, V. G. Zakrzewski, G. A. Voth, P. Salvador, J. J. Dannenberg, S. Dapprich, A. D. Daniels, O. Farkas, J. B. Foresman, J. V. Ortiz, J. Cioslowski, D. J. Fox. Gaussian, Inc., Wallingford, CT (2013).
[50] G. Petsis, Z. Salta, A. M. Kosmas, O. N. Ventura. *Int. J. Quantum. Chem.* **119**, 17 (2019).
[51] E. Maimon, U. Samuni, S. Goldstein. *Radiat. Phys. Chem.* **143**, 14 (2018).